RSC Advances

PAPER

View Article Online
View Journal | View Issue

Cite this: *RSC Adv.*, 2017, **7**, 27969

Large-area synthesis of monolayer $MoSe_2$ films on SiO_2/Si substrates by atmospheric pressure chemical vapor deposition

Yu Zhao,[ab] Hyunjea Lee,[c] Woong Choi,*[d] Weidong Fei[b] and Cheol Jin Lee *[ac]

Received 29th March 2017
Accepted 19th May 2017

DOI: 10.1039/c7ra03642f

rsc.li/rsc-advances

We report the synthesis of large-scale continuous $MoSe_2$ films on SiO_2/Si substrates by atmospheric pressure chemical vapor deposition (CVD). As-grown thin films were composed of a continuous monolayer of $MoSe_2$ and extended up to a millimeter scale. The CVD-grown monolayer $MoSe_2$ films were uniform in thickness and highly crystalline with hexagonal crystal structures. Raman and photoluminescence spectra showed that CVD-grown monolayer $MoSe_2$ films have similar vibrational and optical properties to those of mechanically exfoliated monolayer $MoSe_2$. These results demonstrate that the CVD-grown monolayer $MoSe_2$ films have reasonably high quality comparable to that of mechanically exfoliated monolayer $MoSe_2$ flakes.

Introduction

In recent years, transition metal dichalcogenides (TMDs) with an atomically thin two-dimensional layer structure have attracted enormous attention because of their excellent electronic and optical properties.[1–8] The band gap of TMDs semiconductors (1–2 eV) makes them promising candidates for the channel materials of field-effect transistors (FETs).[9–11] Moreover, TMDs materials such as MoS_2 or $MoSe_2$ show indirect-to-direct bandgap transition when their thickness decreases down to monolayer.[12,13] This suggests that monolayer TMDs semiconductors are very promising for potential applications in optoelectronic devices such as photo detectors.[14,15]

So far, various methods have been tried to obtain large-area TMDs films as the synthesis of large-area TMDs is one of the critical challenges for their real applications. Most emphasis has been put on MoS_2. Mechanical exfoliation provides high-quality crystalline flakes. But, their size is limited, the number of layer is uncontrollable, and the product yield is very low.[4,16,17] Chemical exfoliation and electrochemical exfoliation provide a simple and easy way but obtained flakes are small in the size and uncontrollable in thickness.[18,19] Sulfurization of transition metals or transition metal oxides provides large-area films, but obtained films show uncontrollable thickness uniformity.[20] In comparison, chemical vapor deposition (CVD) with solid-phase precursors (such as S and MoO_3 powder) can provide an effective method to synthesize monolayer MoS_2 with reasonable quality on different substrates including SiO_2/Si wafers, metal foils, or sapphire wafers.[21–24] Moreover, CVD with metalorganic (MO) precursors can provide wafer-scale continuous MoS_2 films.[25]

The use of $MoSe_2$ could be more suitable than MoS_2 for the application of tunnel FETs, optoelectronic devices and spintronic devices with its narrower bandgap,[13] higher optical absorbance[26] and larger spin-splitting energy[27] than MoS_2. However, compared to CVD-grown monolayer MoS_2, there have been much less reports on CVD-grown monolayer $MoSe_2$.[28–37] Thin films of $MoSe_2$ has not yet been obtained by CVD with MO precursors. Furthermore, it is much more difficult to synthesize monolayer $MoSe_2$ films by CVD with solid-phase precursors than monolayer MoS_2 films because of the low chemical reactivity of Se. CVD with solid-phase precursors commonly results in triangular-shaped discontinuous domains of either single-layer $MoSe_2$ or mixtures of single- and few-layer $MoSe_2$.[28–30,32–35,37] While continuous thin films of monolayer $MoSe_2$ can be obtained on substrates up to about 1 cm^2 in size by meticulously tuning and optimizing experimental parameters of low pressure CVD processes,[36] continuous $MoSe_2$ films with such size have not yet been reported by atmospheric pressure CVD. As atmospheric pressure CVD can allow higher deposition rate and lower substrate temperature than low pressure CVD in general, it is still of interest to synthesize large-area $MoSe_2$ films with a uniform thickness by atmospheric pressure CVD. Here, we demonstrate the synthesis of large-area monolayer $MoSe_2$ films extended up to a millimeter scale on SiO_2/Si substrates by atmospheric pressure CVD. The obtained monolayer $MoSe_2$ shows very uniform film thickness, good continuity, highly crystalline hexagonal crystal structures.

[a]*Department of Micro/Nano Systems, Korea University, Seoul 02841, Korea. E-mail: cjlee@korea.ac.kr*

[b]*School of Materials Science and Engineering, Harbin Institute of Technology, Harbin 150001, PR China*

[c]*School of Electrical Engineering, Korea University, Seoul 02841, Korea*

[d]*School of Advanced Materials Engineering, Kookmin University, Seoul 02707, Korea. E-mail: woongchoi@kookmin.ac.kr*

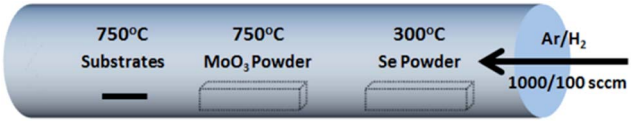

Fig. 1 Schematic illustration for the growth of $MoSe_2$ films on a SiO_2/Si substrate by CVD.

Furthermore, we compare for the first time the vibrational and optical properties of monolayer $MoSe_2$ thin films to those of mechanically exfoliated monolayer $MoSe_2$ single crystals.

Experimental

The schematic illustration of the synthesis of $MoSe_2$ films is shown in Fig. 1. The atmospheric pressure CVD reaction was carried out using a two-zone horizontal tube furnace with a one inch diameter quartz tube. Se powder was loaded in an alumina boat at the center of zone 1, and MoO_3 powder was loaded in an alumina boat at the center of zone 2. A 300 nm-SiO_2/Si substrate was located at the center of zone 2 with its face down on another alumina boat. During the synthesis of $MoSe_2$ film, zone 1 was heated to 300 °C with flowing Ar/H_2 carrier gases under atmospheric pressure while zone 2 was heated to 750 °C. The Ar and H_2 flow rates were 1500 sccm and 150 sccm, respectively. Se powder was evaporated at the center of zone 1 and transported to zone 2 downstream by Ar carrier gas, and MoO_3 powder was reduced by H_2 gas at the same time. The selenization of vapor-phase Mo produced nucleation of $MoSe_2$ species on the SiO_2/Si substrate. Finally, the nucleated $MoSe_2$ species grew into large-area $MoSe_2$ films. It is well understood that hydrogen plays a critical role in the growth of $MoSe_2$ films as an additional reducing agent with Se and MoO_3 powder precursors.[30,38] $MoSe_2$ films were not observed on the substrates without H_2 gas.

Results and discussion

Fig. 2(a)–(d) show the optical images of as-grown $MoSe_2$. The area covered with monolayer $MoSe_2$ looks dark while uncovered area looks bright. The monolayer $MoSe_2$ films with several hundred micrometers were found on SiO_2/Si substrates as shown in Fig. 2(a) and (b) (we intentionally scratched the surface to leave the pink colored line). Fig. 2(c) shows some triangular domains of $MoSe_2$ with several micrometers on SiO_2/Si substrates. Those domains merge together and become a continuous and large-area film up to several hundred micrometers. Partly some triangular domains are folded, resulting in bilayers or triple layers as shown in Fig. 2(d). The homogeneous color of $MoSe_2$ films in optical images suggests that the as-grown $MoSe_2$ films have good continuity and uniformity. Atomic force microscopy (AFM) was used to measure the morphology and the thickness of the $MoSe_2$ films. Fig. 2(e) and (f) show the AFM image and the height of as-grown $MoSe_2$ film on the SiO_2/Si substrate, respectively. The measured height is about 0.7 nm, which is consistent with the thickness of mechanically exfoliated monolayer $MoSe_2$ flakes.

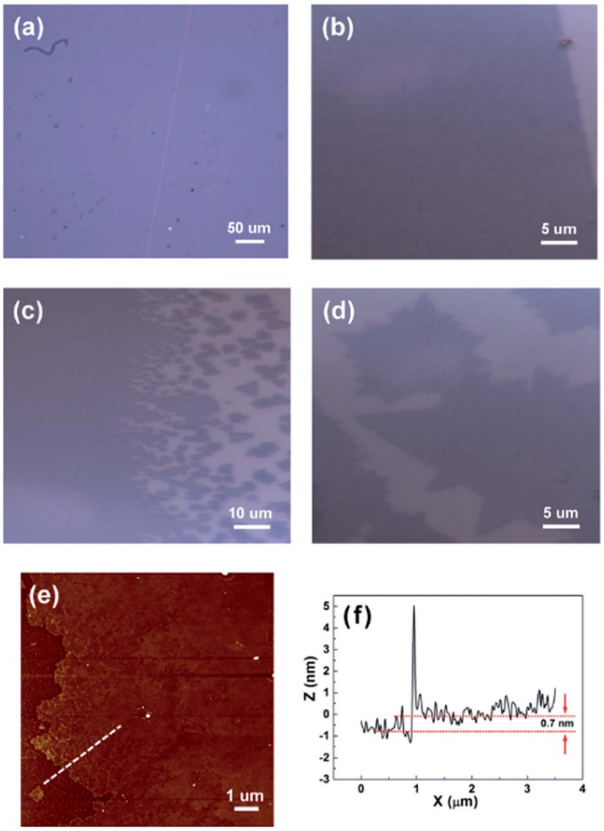

Fig. 2 (a–d) Optical images of the as-grown monolayer $MoSe_2$ film. (e) AFM image of the as-grown $MoSe_2$ film. (f) Height profile of the $MoSe_2$ film obtained from the corresponding white line shown in (e).

Raman spectrum is an effective method to characterize layer numbers of TMDs materials. Fig. 3(a) shows the Raman spectra of as-grown mono-, bi-, and multilayer $MoSe_2$ films with

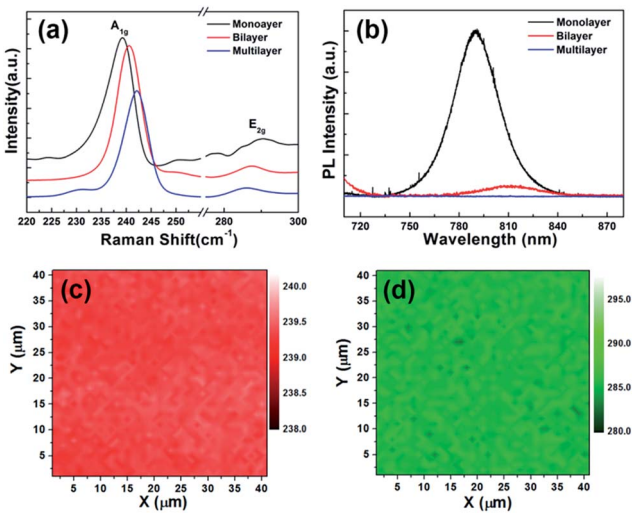

Fig. 3 (a) Raman spectra of $MoSe_2$ films with different number of layers. (b) Photoluminescence (PL) spectra of $MoSe_2$ with different number of layers. (c) Raman mapping of the monolayer $MoSe_2$ film (A_{1g} mode). (d) Raman mapping of the monolayer $MoSe_2$ film (E_{2g} mode).

a 514 nm excitation laser. There are two main peaks in the Raman spectra, one is a sharp peak at low wavenumber corresponding to A_{1g} mode (out of plane vibration), and another is a broad peak at high wavenumber corresponding to E_{2g} mode (in plane vibration). In general, the location of Raman modes can be used to determine the thickness of TMDs materials. In this work, the A_{1g} and E_{2g} modes of monolayer $MoSe_2$ films are located at 239.2 and 290.3 cm^{-1}, respectively, which is well agreed with the previous results of 2H-phase exfoliated monolayer $MoSe_2$ flakes and CVD-grown monolayer $MoSe_2$ films.[12,33] As the thickness of $MoSe_2$ film increases from monolayer to multilayer, the A_{1g} mode is blue-shifted to 240.2 cm^{-1}, and the E_{2g} mode is red-shifted to 285.9 cm^{-1}. Similar results were also previously reported by other groups.[15,30,32,33]

In order to confirm the bandgap of CVD-grown $MoSe_2$ films, photoluminescence (PL) spectra were measured. Fig. 3(b) shows the PL spectra of mono-, bi-, and multilayer $MoSe_2$ films. A monolayer $MoSe_2$ film shows a high intensity peak at 790 nm (1.57 eV), which can be ascribed to the direct bandgap at *K* point of Brillouin zone.[13] The observed PL emission at 1.57 eV is in good agreement with the reported values in literature.[32,33] The bandgap of $MoSe_2$ changes from direct to indirect as the thickness increases from monolayer to multilayer. This significantly decreases PL peak intensity.[13] The PL peak of bilayer $MoSe_2$ films is red-shifted to 810 nm (1.53 eV), and the peak intensity is approximately 15 times weaker than that of monolayer $MoSe_2$ films. This is also in good agreement with the results on $MoSe_2$ bilayer in literature.[33] Moreover, it is difficult to find noticeable peak intensity for multilayer $MoSe_2$ films.

It is well known that Raman mapping can further confirm uniformity and continuity of the CVD-grown $MoSe_2$ films. Fig. 3(c) and (d) show Raman mapping of monolayer $MoSe_2$ films in the area of 40 × 40 μm^2 where the distribution in A_{1g} and E_{2g} mode is presented, respectively. The uniform color of the two mapping images indicates that the CVD-grown $MoSe_2$ films have considerably good uniformity and continuity. Raman and PL analysis suggests that our CVD-grown monolayer $MoSe_2$ films are uniform in thickness.

In order to investigate elemental composition and binding energy of the as-grown monolayer $MoSe_2$ films, X-ray photoelectron spectroscopy (XPS) was used. Carbon binding energy was set as a reference to remove any effects of charge accumulation on these samples, and the backgrounds were estimated as Shirley-type.[28] Fig. 4(a) shows that $MoSe_2$ films have the binding energy of 229.1 and 232.2 eV at Mo $3d_{5/2}$ and $3d_{3/2}$ peaks, respectively. In this work, the binding energies of Mo are significantly shifted from those of hexavalent Mo (~232.5 and 235.9 eV), suggesting the reduction of Mo from Mo^{6+} (MoO_3) to Mo^{4+}.[39] Fig. 4(b) shows the binding energies of 54.5 and 55.3 eV corresponding to divalent Se ions (Se $3d_{5/2}$ and $3d_{3/2}$, respectively). It is worth noting that XPS results are consistent with previous works in literature confirming the chemical valence states of the CVD-grown monolayer $MoSe_2$ films.[28,31]

The crystal structure of CVD-grown monolayer $MoSe_2$ films was characterized using transmission electron microscopy (TEM). The $MoSe_2$ films were transferred to a carbon-coated Cu TEM grid. Fig. 5(a) shows that the transferred $MoSe_2$ film has good continuity but some folds and small particles exist due to residual organics or unskillful transfer technique. Fig. 5(b) shows a triangular grain with several micrometers in size inside a continuous $MoSe_2$ film, indicating the polycrystalline nature of CVD-grown monolayer $MoSe_2$ films. Fig. 5(c) shows a TEM image of a monolayer $MoSe_2$ film with a corresponding fast Fourier transformation (FFT) pattern in the inset. The FFT pattern exhibits clear six-fold

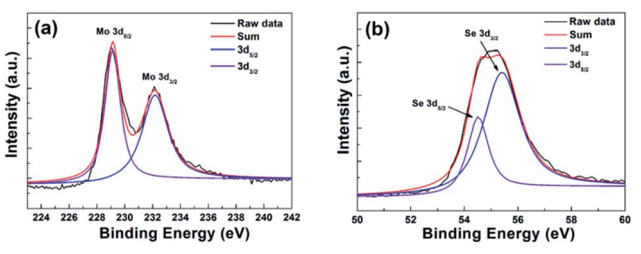

Fig. 4 XPS characterization of monolayer $MoSe_2$ film. (a) XPS spectra of Mo 3d binding energy and (b) XPS spectra of Se 3d binding energy.

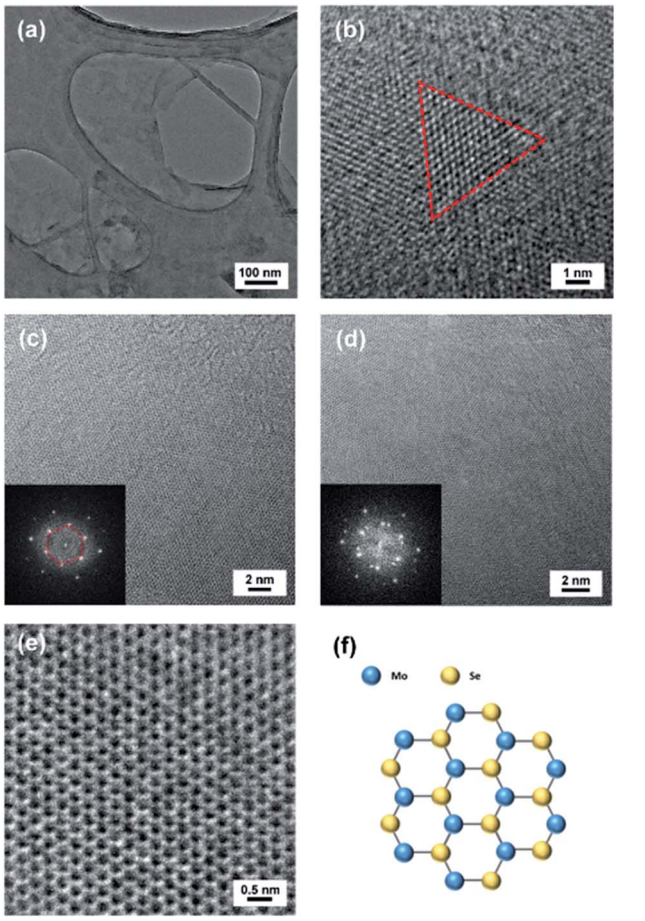

Fig. 5 TEM characterization of the sample. (a) TEM image of a CVD-grown monolayer $MoSe_2$ film transferred onto a TEM grid. The folds were produced during the transfer onto the grid. (b) Magnified TEM image of a monolayer $MoSe_2$ film. The dot line indicates a triangular grain. (c) TEM image of a monolayer $MoSe_2$ film with its corresponding FTT (inset). (d) TEM image of a bilayer $MoSe_2$ film with its corresponding FTT (inset). (e) HRTEM image of a monolayer $MoSe_2$ film. (f) Schematics illustrating the atomic structure of $MoSe_2$.

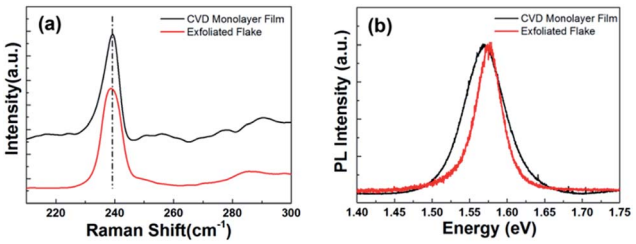

Fig. 6 (a) Raman spectra of the mechanically exfoliated monolayer $MoSe_2$ flake and the CVD-grown monolayer $MoSe_2$ film. (b) Photoluminescence (PL) spectra of the mechanically exfoliated monolayer $MoSe_2$ flake and CVD-grown monolayer $MoSe_2$ film.

symmetry of diffraction spots, demonstrating single layer $MoSe_2$ film with a hexagonal structure. Fig. 5(d) shows a TEM image of a bilayer $MoSe_2$ film with a corresponding FFT pattern in the inset. The FFT pattern indicates a twist between two layers with additional six diffraction spots. Fig. 5(e) clearly demonstrates the expected hexagonal crystal structure of monolayer $MoSe_2$ in the high resolution TEM (HRTEM) image. The lattice constant is ~0.3 nm, which is well agreed with the previous results of monolayer $MoSe_2$.[28,30,31,33] HRTEM images and FFT patterns confirm the high crystallinity of the CVD-grown monolayer $MoSe_2$ films.

It needs to be mentioned that, while perfect 2H-phase MoS_2 is known to be inert, defects such as vacancies and grain boundaries in real MoS_2 can lead to poor long-term stability in air.[40,41] As a theoretical calculation predicts comparable oxidation behavior between single layer MoS_2 and $MoSe_2$,[40] we expect our CVD-grown $MoSe_2$ thin films could be more resistant to oxidation with improved crystallinity in the future.

Finally, the quality of the CVD-grown monolayer $MoSe_2$ film was compared to a mechanically exfoliated monolayer $MoSe_2$ flake through Raman and PL spectra. Fig. 6(a) shows that Raman spectrum of CVD-grown monolayer $MoSe_2$ film is consistent with that of an exfoliated monolayer $MoSe_2$ flake, which indicates the high quality of the CVD-grown monolayer $MoSe_2$ film. Even though the PL spectrum in Fig. 6(b) shows that the emission peak of CVD-grown monolayer $MoSe_2$ film exhibits very similar intensity and energy to those of the mechanically exfoliated monolayer $MoSe_2$ flake, the CVD-grown monolayer $MoSe_2$ film shows a slightly wider full-width at half-maximum of PL peak than that of the mechanically exfoliated monolayer $MoSe_2$ flake. It may imply that the CVD-grown monolayer $MoSe_2$ film has a little higher defect density than that of the mechanically exfoliated monolayer $MoSe_2$ flake. In fact, the interpretation of the crystal quality by optical analysis like Raman or PL is complicated to assess the crystal quality of two-dimensional materials.[42] Nevertheless, these results suggest that the CVD-grown monolayer $MoSe_2$ film has reasonably high quality comparable to that of the mechanically exfoliated monolayer $MoSe_2$ flake.

Conclusions

We investigated the synthesis of large-area monolayer $MoSe_2$ films on SiO_2/Si substrates by atmospheric pressure CVD. The CVD-grown monolayer $MoSe_2$ exhibited continuous and large-scale films with uniform thickness. The HRTEM images with corresponding FFT patterns revealed that CVD-grown monolayer $MoSe_2$ films have hexagonal crystal structure with high crystallinity. Raman and PL spectra analysis showed that the CVD-grown monolayer $MoSe_2$ films have comparable vibrational and optical properties with those of mechanically-exfoliated monolayer $MoSe_2$ flakes. These results demonstrate that our large-area CVD-grown monolayer $MoSe_2$ films have reasonably high quality comparable to that of the mechanically exfoliated monolayer $MoSe_2$ flake. We suggest that our large-area and high quality CVD-grown monolayer $MoSe_2$ films can expand understanding on the synthesis of TMDs materials, providing potentially important implications on their applications in various electronic and photonic devices in the future.

Acknowledgements

This work was supported by Brain Korea 21 Plus Project (T1300304) and Carbon-based Technology for the Internet-of-Things Era Project (K1518861).

References

1 A. Splendiani, L. Sun, Y. Zhang, T. Li, J. Kim, C. Y. Chim, G. Galli and F. Wang, *Nano Lett.*, 2010, **10**, 1271–1275.
2 B. Radisavljevic, A. Radenovic, J. Brivio, V. Giacometti and A. Kis, *Nat. Nanotechnol.*, 2011, **6**, 147–150.
3 G. Eda, H. Yamaguchi, D. Voiry, T. Fujita, M. Chen and M. Chhowalla, *Nano Lett.*, 2011, **11**, 5111–5116.
4 Q. H. Wang, K. Kalantar-Zadeh, A. Kis, J. N. Coleman and M. S. Strano, *Nat. Nanotechnol.*, 2012, **7**, 699–712.
5 W. Choi, M. Y. Cho, A. Konar, J. H. Lee, G. B. Cha, S. C. Hong, S. Kim, J. Kim, D. Jena, J. Joo and S. Kim, *Adv. Mater.*, 2012, **24**, 5832–5836.
6 S. Kim, A. Konar, W.-S. Hwang, J. H. Lee, J. Lee, J. Yang, C. Jung, H. Kim, J.-B. Yoo, J.-Y. Choi, Y. W. Jin, S. Y. Lee, D. Jena, W. Choi and K. Kim, *Nat. Commun.*, 2012, **3**, 1011.
7 H. Kwon, W. Choi, D. Lee, Y. Lee, J. Kwon, B. Yoo, C. P. Grigoropoulos and S. Kim, *Nano Res.*, 2014, **7**, 1137–1145.
8 H. T. Mohammad and J. S. Volker, *Nanotechnology*, 2015, **26**, 344005.
9 O. Lopez-Sanchez, D. Lembke, M. Kayci, A. Radenovic and A. Kis, *Nat. Nanotechnol.*, 2013, **8**, 497–501.
10 B. Chamlagain, Q. Li, N. J. Ghimire, H.-J. Chuang, M. M. Perera, H. Tu, Y. Xu, M. Pan, D. Xaio, J. Yan, D. Mandrus and Z. Zhou, *ACS Nano*, 2014, **8**, 5079–5088.
11 D. Ovchinnikov, A. Allain, Y.-S. Huang, D. Dumcenco and A. Kis, *ACS Nano*, 2014, **8**, 8174–8181.
12 K. F. Mak, C. Lee, J. Hone, J. Shan and T. F. Heinz, *Phys. Rev. Lett.*, 2010, **105**, 136805.
13 S. Tongay, J. Zhou, C. Ataca, K. Lo, T. S. Matthews, J. Li, J. C. Grossman and J. Wu, *Nano Lett.*, 2012, **12**, 5576–5580.
14 H. R. Gutiérrez, N. Perea-López, A. L. Elías, A. Berkdemir, B. Wang, R. Lv, F. López-Urías, V. H. Crespi, H. Terrones and M. Terrones, *Nano Lett.*, 2013, **13**, 3447–3454.

15 P. Tonndorf, R. Schmidt, P. Bottger, X. Zhang, J. Borner, A. Liebig, M. Albrecht, C. Kloc, O. Gordan, D. R. T. Zahn, S. M. de Vasconcellos and R. Bratschitsch, *Opt. Express*, 2013, **21**, 4908–4916.

16 H. Li, J. Wu, Z. Yin and H. Zhang, *Acc. Chem. Res.*, 2014, **47**, 1067–1075.

17 M. Chhowalla, H. S. Shin, G. Eda, L.-J. Li, K. P. Loh and H. Zhang, *Nat. Chem.*, 2013, **5**, 263–275.

18 J. N. Coleman, M. Lotya, A. O'Neill, S. D. Bergin, P. J. King, U. Khan, K. Young, A. Gaucher, S. De, R. J. Smith, I. V. Shvets, S. K. Arora, G. Stanton, H. Y. Kim, K. Lee, G. T. Kim, G. S Duesberg, T. Hallam, J. J. Boland, J. J. Wang, J. F. Donegan, J. C. Grunlan, G. Moriarty, A. Shmeliov, R. J. Nicholls, J. M. Perkins, E. M. Grieveson, K. Theuwissen, D. W. McComb, P. D. Nellist and V. Nicolosi, *Science*, 2011, **331**, 568–571.

19 Z. Zeng, Z. Yin, X. Huang, H. Li, Q. He, G. Lu, F. Boey and H. Zhang, *Angew. Chem., Int. Ed.*, 2011, **50**, 11093–11097.

20 Y.-C. Lin, W. Zhang, J.-K. Huang, K.-K. Liu, Y.-H. Lee, C.-T. Liang, C.-W. Chu and L.-J. Li, *Nanoscale*, 2012, **4**, 6637–6641.

21 Y.-H. Lee, L. Yu, H. Wang, W. Fang, X. Ling, Y. Shi, C.-T. Lin, J.-K. Huang, M.-T. Chang, C.-S. Chang, M. Dresselhaus, T. Palacios, L.-J. Li and J. Kong, *Nano Lett.*, 2013, **13**, 1852–1857.

22 J. Shi, D. Ma, G.-F. Han, Y. Zhang, Q. Ji, T. Gao, J. Sun, X. Song, C. Li, Y. Zhang, X.-Y. Lang, Y. Zhang and Z. Liu, *ACS Nano*, 2014, **8**, 10196–10204.

23 L. Ma, D. N. Nath, E. W. Lee, C. H. Lee, M. Yu, A. Arehart, S. Rajan and Y. Wu, *Appl. Phys. Lett.*, 2014, **105**, 072105.

24 W. Shanshan, P. Merce, B. Harish and H. W. Jamie, *Nanotechnology*, 2016, **27**, 085604.

25 K. Kang, S. Xie, L. Huang, Y. Han, P. Y. Huang, K. F. Mak, C.-J. Kim, D. Muller and J. Par, *Nature*, 2015, **520**, 656–660.

26 M. Bernardi, M. Palummo and J. C. Grossman, *Nano Lett.*, 2013, **13**, 3664.

27 Y. Zhang, T.-R. Chang, B. Zhou, Y.-T. Cui, H. Yan, Z. Liu, F. Schmitt, J. Lee, R. Moore, Y. Chen, H. Lin, H.-T. Jeng, S.-K. Mo, Z. Hussain, A. Bansil and Z.-X. Shen, *Nat. Nanotechnol.*, 2014, **9**, 111.

28 Y. H. Chang, W. Zhang, Y. Zhu, Y. Han, J. Pu, J. K. Chang, W. T. Hsu, J. K. Huang, C. L. Hsu, M. H. Chiu, T. Takenobu, H. Li, C. I. Wu, W. H. Chang, A. T. S. Wee and L. J. Li, *ACS Nano*, 2014, **8**, 8582–8590.

29 A. Bachmatiuk, R. F. Abelin, H. T. Quang, B. Trzebicka, J. Eckert and M. H. Rummeli, *Nanotechnology*, 2014, **25**, 365603.

30 J. Shaw, H. Zhou, Y. Chen, N. Weiss, Y. Liu, Y. Huang and X. Duan, *Nano Res.*, 2014, **7**, 511–517.

31 X. Wang, Y. Gong, G. Shi, W. L. Chow, K. Keyshar, G. Ye, R. Vajtai, J. Lou, Z. Liu, E. Ringe, B. K. Tay and P. M. Ajayan, *ACS Nano*, 2014, **8**, 5125–5131.

32 X. Lu, M. I. B. Utama, J. H. Lin, X. Gong, J. Zhang, Y. Y. Zhao, S. T. Pantelides, J. X. Wang, Z. L. Dong, Z. Liu, W. Zhou and Q. H. Xiong, *Nano Lett.*, 2014, **14**, 2419–2425.

33 J. Xia, X. Huang, L.-Z. Liu, M. Wang, L. Wang, B. Huang, D.-D. Zhu, J.-J. Li, C.-Z. Gu and X.-M. Meng, *Nanoscale*, 2014, **6**, 8949–8955.

34 G. W. Shim, K. Yoo, S.-B. Seo, J. Shin, D. Y. Jung, I.-S. Kang, C. W. Ahn, B. J. Cho and S.-Y. Choi, *ACS Nano*, 2014, **8**, 6655–6662.

35 C. Jung, S. M. Kim, H. Moon, G. Han, J. Kwon, Y. K. Hong, I. Omkaram, Y. Yoon, S. Kim and J. Park, *Sci. Rep.*, 2015, **5**, 15313.

36 Y. Gong, G. Ye, S. Lei, G. Shi, Y. He, J. Lin, X. Zhang, R. Vajtai, S. T. Pantelides, W. Zhou, B. Li and P. M. Ajayan, *Adv. Funct. Mater.*, 2016, **26**, 2009–2015.

37 H. Liu, Z. Chen, X. Chen, S. Chu, J. Huang and R. Peng, *J. Mater. Chem. C*, 2016, **4**, 9399–9404.

38 J.-K. Huang, J. Pu, C.-L. Hsu, M.-H. Chiu, Z.-Y. Juang, Y. H. Chang, W.-H. Chang, Y. Iwasa, T. Takenobu and L.-J. Li, *ACS Nano*, 2014, **8**, 923–930.

39 M. Bougouma, A. Batan, B. Guel, T. Segato, J. B. Legma, F. Reniers, M.-P. Delplancke-Ogletree, C. Buess-Herman and T. Doneux, *J. Cryst. Growth*, 2013, **363**, 122–127.

40 H. Liu, N. Han and J. Zhao, *RSC Adv.*, 2015, **5**, 17572–17581.

41 J. Gao, B. Li, J. Tan, P. Chow, T.-M. Lu and N. Koratkar, *ACS Nano*, 2016, **10**, 2628–2635.

42 S. Tongay, J. Suh, C. Ataca, W. Fan, A. Luce, J. S. Kang, J. Liu, C. Ko, R. Raghunathanan, J. Zhou, F. Ogletree, J. B. Li, J. C. Grossman and J. Wu, *Sci. Rep.*, 2013, **3**, 2657.